Drought hazard transferability from meteorological to hydrological propagation

Lei Gu[1], Jie Chen[1, 2*], Jiabo Yin[1], Chong-Yu Xu[1, 3], Hua Chen[1]

[1]State Key Laboratory of Water Resources and Hydropower Engineering Science, Wuhan University, Wuhan 430072, P. R. China

[2]Hubei Provincial Key Lab of Water System Science for Sponge City Construction, Wuhan University, Wuhan, China

[3]Department of Geosciences, University of Oslo, P.O. Box 1047 Blindern, N-0316 Oslo, Norway

* Corresponding author, Email: jiechen@whu.edu.cn

Abstract

As a major weather-driven disaster, drought can be assessed from meteorological to hydrological aspects. Although the propagation from meteorological to hydrological droughts has received lots of attention in recent years, the hazard transferability in such a propagation process has been less investigated. In this study, we propose a framework with the incorporation of copulas and a drought hazard propagation ratio (DHPR) to examine the drought propagation process, particularly to investigate the accompanying hazard transferability. Three catchments with few human activities located in two major river basins of China (i.e., the Yangtze River basin and the Yellow River basin) with different hydro-climatic conditions are selected as case studies. First, the standardized precipitation evapotranspiration index (SPEI) and the standardized runoff index (SRI) are calculated to measure meteorological and hydrological droughts for the 1961-2014 period. Subsequently, the drought duration and severity are identified using the theory of run, and then the most-likely scenarios and the corresponding uncertainty ellipse based on copulas are incorporated to appraise meteorological and hydrological drought hazards. Finally, a novel concept of DHPR is proposed to evaluate the hazard transferability from meteorological to hydrological drought. The results show that (1) the drought propagation generally shows lengthened duration, amplified severity, and the time-delay phenomenon among these catchments; (2) drought hazards represented by the most-likely scenarios of duration and severity and the uncertainty ellipse tend to ascend based on the bivariate frequency analysis; and (3) the hazard transferability is stable from meteorological to hydrological droughts, as indicated by the almost unchanged DHPR ranging between 1 and 2 for the most-likely scenarios and varying between 2 and 4 for the uncertainty ellipse under different return periods. The above results imply firm and robust correlations between meteorological and hydrological drought hazards, which can provide a supplement for revealing the drought propagation mechanism and would benefit drought risk assessment.

Keywords: Meteorological drought; hydrological drought; drought propagation; drought return period; most-likely events;

1 Introduction

As one of the most complex and severe natural hazards, drought has widespread impacts on society and the environment. Depending on the considered hydro-climatic variables and impacted aspects, drought can be defined as meteorological drought, hydrological drought, agricultural drought, and socio-economic drought (Mishra et al., 2010). From the perspective of social activities on water resources, such as irrigation, industry and urban water supply, meteorological and hydrological droughts, defined as an abnormally dry climate and a deficit in surface or subsurface water, respectively, can be the most important (Haslinger et al., 2014; Su et al., 2018). Understanding the links between meteorological and hydrological droughts is necessary for revealing the causative mechanism of droughts, and is of paramount importance in water resource planning and management.

Previous studies (e.g. Huang et al., 2017; Apurv et al., 2017; Guo et al., 2020) have investigated the links between meteorological and hydrological droughts in recent years and classified them into three categories. The first category involves analyzing the correlations between hydrological and meteorological droughts combined with the investigation of contributing factors (Lorenzo-Lacruz et al., 2013; Vicente-Serrano et al., 2005). For example, Folland et al. (2015) used the standardized indicators to reflect temporal correlations among meteorological drought (i.e., Standardized Precipitation Index, SPI) and streamflow drought (i.e., Standardized Streamflow Index, SSI), and found high correlations exist between them. Haslinger et al. (2014) investigated their correlations by using rank correlation analysis and found that there was a significant correlation between hydrological drought and meteorological drought under humid conditions. However, this correlation can be weakened to some extent under a dry climate, especially for catchments where groundwater storage and snow processes are significant. Overall, the above studies demonstrate that there are non-negligible correlations between meteorological droughts and their manifestation in hydrological responses, though the intensity of these correlations varies with local or regional climatic and underlying surface conditions (Barker et al., 2016).

The second category focuses on investigating the variations of drought characteristics (e.g., frequency, duration, severity and area) across typical events in meteorological and hydrological conditions by using modeling or statistical approaches (Yang et al., 2017; Zhang et al., 2017). For instance, Vidal et al. (2010) identified meteorological and hydrological droughts over France and found that mean duration and severity of hydrological droughts appeared to be larger than that of meteorological droughts, but a reversed pattern in drought propagation processes can also be detected across some particular events and regions. Liu et al. (2019) established a multivariate joint distribution of duration, severity and area to connect meteorological and hydrological drought events, and concluded that minor meteorological droughts were less prone to result in a hydrological response. They also found that lagging and lengthening features exist in the propagation of the drought signal from meteorological to hydrological drought. Van Loon et al. (2015) used an Austrian dataset consisting of 44 catchments to investigate drought propagation. They found that there were fewer but longer droughts in discharge than in precipitation, and found that the average deficit volume of droughts in discharge was comparable with that in precipitation, though with larger ranges. In brief, previous studies witness the responses of hydrological droughts to meteorological droughts and the comparability with regard to their characteristics.

The third category mainly involves using meteorological drought indices to detect hydrological droughts to solve problems in the absence of hydrological records (e.g., Zhai et al., 2010; Wong, 2013; Hao et al., 2015). For example, Zhu et al. (2016) proposed an approach by combining meteorological indices at multiple timescales to monitor hydrological droughts. They indicated that meteorological indices (e.g., SPI) of short timescales (1-3 months) performed better in detecting hydrological droughts with short duration and deficit, whereas indices of long timescales, especially blended timescales (e.g., blending 8-month SPEI and 9-month SPEI), are more robust in detecting extremely severe hydrological droughts.

Although previous studies have investigated the variations of drought indicators and characteristics, no work has studied the variations of drought hazards propagating from the anomalous dry climates to the terrestrial part of the hydrological cycle. In general, a hazard quantifies the probability of the occurrence of a potentially damaging phenomenon. It represents a probability ranging between 0 and 1, and is usually denoted by a return period. Variations of drought indicators and characteristics can apparently result in changes of drought hazards, which is crucial for effective drought monitoring and management (Gu et al., 2020; Dai et al., 2020). From this perspective, quantifying the variations of drought hazards can help to understand drought propagation mechanisms, as well as benefiting drought mitigation and adaptation strategies.

Over the years, a suite of approaches has been developed to investigate drought hazards, and especially for multivariate probabilistic characterization of droughts. The copula-based methodology for multivariate frequency analyses has been well established in drought fields. For example, Zhang et al. (2015) estimated regional joint probability and the uncertainty of joint probability curves in terms of drought duration and severity in China by using the fuzzy c-means method and copula functions. Ayantobo et al. (2018) employed bivariate Archimedean copulas to systematically appraise meteorological drought hazards in mainland China for the 1961–2013 period. They found that Northwestern and Southwestern China would subject to the highest drought hazards.

Different from univariate frequency analyses, where a determined design value of drought characteristics can be estimated under a given return period, there are infinite combinations of drought characteristics in the multivariate case. Lack of uniquely determined drought design values may hinder making effective drought management and mitigation polices. In fact, the occurrence probability of these infinite combinations is not the same. The most-likely scenario that has the highest probability of occurrence (the largest joint probability density) among these combinations appears to be the best representative candidate (Salvadori et al., 2011; Yin et al. 2018a, b). Nevertheless, few studies have identified the most-likely scenarios of drought characteristics in multivariate frequency analyses. Moreover, the inevitably large sampling uncertainty due to limited sample size is usually neglected (Cancelliere et al., 2010; Weng et al., 2015; Chang et al., 2016; Zhang et al., 2017; Ayantobo et al., 2018; Gu et al., 2018), though it is prominent in both univariate and multivariate frequency analyses.

Accordingly, the present study aims at investigating the links between meteorological and hydrological droughts from the hazard assessment perspective. To this end, the specific objectives are to (i) investigate meteorological and hydrological drought hazards based on the most-likely scenarios and their corresponding bivariate uncertainty envelopes; and (ii) characterize the transferability of drought hazards in drought propagation from meteorology to hydrology. To achieve this, a general framework is proposed (Figure 1) to characterize drought hazard propagation processes. The case study is conducted over three catchments with different hydro-climatic conditions, two of which are seasonally snow-covered and the other is driven by subtropical monsoon rainfall. The SPEI and SRI are used to derive meteorological and hydrological droughts, respectively. The hazard transferability is evaluated by comparing both most-likely scenarios and their corresponding uncertainty.

[Please insert Fig. 1 here]

2 Study Area and Data

Three catchments from China's two main river basins were selected to demonstrate the hazard variations between meteorological and hydrological droughts. They include the upper stream of the Yellow River basin (UYRB), and the Jinsha River basin (JSRB) and Jialing River Basin (JLRB) in the Yangtze River basin. The reason to choose these three catchments is because they are less influenced by human activities. The different hydro-climatic characteristics and drainage areas are other reasons to select these catchments.

The UYRB has a surface area of 12.19×10^4 km^2 (Fig. 2(a)). The mean annual precipitation for 1961–2014 was 552 mm, with a standard deviation of 56 mm. It belongs to the cool temperature climate zone with the mean annual daily temperature being around −1.75 ℃. Runoff in this catchment is generated as the combination of snowmelt, groundwater recharge and precipitation. The mean annual runoff depth was 172 mm, with large inter-annual variations (the standard deviation was 39.6 mm).

The JSRB is located in the upper stream of the Yangtze River basin (Fig. 2(b)). It has a catchment area of 43.63×10^4 km^2 and ranges from a cool temperate climate to a monsoon climate. The mean annual precipitation in this catchment was slightly higher than that of the UYRB, with a value of 685 mm (the standard deviation was 48.9 mm). The mean annual daily temperature was 2.89 ℃ with the standard deviation being

0.60 ℃. Both the snowmelt and precipitation contribute to runoff. The mean annual runoff was 329 mm with a standard deviation of 53.5 mm.

The JLRB has a surface area of 15.10 × 10^4 km^2 (Fig. 2(c)). It is located in the upper stream of the Yangtze River basin and has a subtropical monsoon climate. The mean daily temperature was 12.6 ℃, which is much higher than the other two catchments. The water resources in this watershed are the most abundant compared to the other two catchments and the main contributor to runoff is precipitation. The mean annual precipitation was 849 mm with a standard deviation of 93.5 mm, and the mean annual runoff was 437 mm with a standard deviation of 110 mm. The location of the three catchments and corresponding hydrometric stations are shown in Figure 2.

[Please insert Fig. 2 here]

Precipitation data with spatial resolution of 0.5°×0.5° are provided by the China Meteorological Data Sharing Service System (http://www.cma.gov.cn) for these three catchments. Six climate variables (maximum, minimum, and mean air temperature, wind speed, relative humidity, sunshine hours) at the daily scale are used to calculate the potential evapotranspiration (PET). These variables for the period 1961–2014 are collected from 6 gauges in the UYRB, 15 gauges in the JSRB, and 10 gauges in the JLRB. They are then aggregated to monthly values to estimate drought indices. Monthly runoff records covering the 1961–2014 period for the UYRB and JLRB and the 1961-2011 period for the JSRB is provided by the Yangtze River Water Resources Commission and the Yellow River Water Resources Commission in China for the outlet of each catchment, respectively (Tang- Naihai Station, UYRB; Ping-Shan Station, JSRB; and Bei-Pei Station, JLRB).

The MOPEX dataset (http://water.usgs.gov/nwis) is also used to test the proposed framework in this study. This dataset contains daily time series of observations of precipitation and discharge, and potential evapotranspiration based on NOAA Evaporation Atlas (Farnsworth et al., 1982; Yin et al., 2019). The MOPEX data are often assumed to only include in-situ observations unaffected by human interferences (Wang et al., 2011). We selected 218 small-scale catchments (ranging in area from 134 to 10375 km^2) with the high data quality.

3 Methodology

3.1 Drought Index Calculation

The Standardized Precipitation Evapotranspiration Index (SPEI) (Vicente-Serrano et al., 2010) and Standardized Runoff Index (SRI) (Shukla, 2008) are employed to measure the dry and wet conditions in terms of both meteorological and hydrological variables, respectively. SPEI and SRI consist of multiple timescales, while the 6-month timescale is selected to consider a relatively long period of abnormally wet/dry conditions and to filter redundant information introduced by too-long timescales (e.g., 12–24 months) (Ayantobo et al., 2018).

The calculation of SPEI-6 is based on the differences between the aggregated 6-month precipitation (P) and 6-month PET. The three-parameter log-logistic probability distribution is usually employed to fit the aggregated 6-month differences between P and PET:

$$F(\mathrm{x}) = [1 + (\frac{\alpha}{x - \lambda})^{\beta}]^{-1} \tag{1}$$

where F(x) means the cumulative distribution function of the log-logistic distribution, and α, β and λ represent the 3 parameters of the distribution. The maximum likelihood estimation (MLE) method (Ahmad et al., 1988) is used to estimate these 3 parameters. The PET is calculated by using the Food and Agriculture Organization of the United Nations (FAO) Penman-Monteith approach (Allen et al., 1998):

$$PET = \frac{0.408\Delta\left(R_n - G\right) + \gamma \frac{900}{T_{mean} + 273} u_2\left(e_s - e_a\right)}{\Delta + \gamma\left(1 + 0.34u_2\right)} \tag{2}$$

where Δ is the slope of saturation vapor pressure vs. air temperature curve (kPa /℃), R_n is the net radiation (MJ/m^2/day), G is the soil heat flux (MJ/m^2/day) and is close to zero at the daily scale, γ is the psychometric constant (kPa/℃), T_{mean} is the daily mean air temperature at 2-m height (℃), u_2 is the mean wind speed at 2-m height (m s^{-1}), and e_s and e_a are saturated and actual vapor pressure (kPa), respectively. They can be obtained using the following equations:

$$e_s = 0.6108 \times e^{\frac{17.27 \times tmp}{tmp + 237.3}} \tag{3}$$

$$e_a = \frac{rhs}{100} \times e_s \tag{4}$$

where rhs is the relative humidity (%), and tmp is temperature (i.e., daily maximum and minimum air temperature). Due to the non-linearity of eq. (3), here the mean saturated vapor pressure derived from the daily maximum and minimum air temperature is used. At the last step, a standardized process is used to calculate the

SPEI-6 values by transforming the fitted log-logistic distribution function $F(x)$ to the standard normal distribution with a mean of zero and a standard deviation of one (Vicente et al-Serrano., 2012; Huang et al., 2017; Gu et al., 2019). The SPEI-6 values are derived as the standardized values of $F(x)$.

SRI-6 is calculated with the similar method to SPEI-6. However, the Person-III distribution recommended by the Chinese Guideline (MWR, 2006) is used to fit the aggregated 6-month runoff series for each calendar end-month (of the 6-month period) (Barker et al., 2016):

$$F(\mathrm{x}) = \frac{\beta^{\alpha}}{\Gamma(\alpha)} \int_{x}^{\infty} (\mathrm{x}-\omega)^{\alpha-1} e^{-\beta(\mathrm{x}-\omega)} dx \tag{5}$$

where $F(\mathrm{x})$ means the cumulative distribution function of the Person-III distribution, and α, β and ω represent the 3 parameters of the distribution.

3.2 Drought Event Identification

A meteorological (hydrological) drought event is defined for values of SPEI-6 (SRI-6) continuously below zero, and a meteorological (hydrological) event ends when the values of SPEI-6 (SRI-6) rise above zero (Yevjevich et al., 1967; Mishra et al., 2010; Zargar et al., 2011; Ayantobo et al., 2017). The duration and severity are then extracted as two measurements to characterize drought events. The drought duration is defined as the length of the time period that the values of SPEI-6 (SRI-6) are continuously negative, and the drought severity is defined as the cumulative SPEI-6 (SRI-6) values in the drought duration (to facilitate analysis, absolute values are used in this study).

3.3 Copula Theory for Drought Analysis

(1) Marginal distribution function for drought analysis

For univariate drought analyses, the Gamma, Normal, Weibull, Log-logistic, Log-normal and Exponential distributions (Kwon et al., 2016) are usually employed to fit drought duration and drought severity. The best distribution is identified by using the Akaike information criterion (AIC) (Bozdogan et al., 1987):

$$AIC = 2\log(\mathrm{MSE}) + \frac{2 \times n \times k}{n-k-1} \tag{6}$$

where log(MSE) denotes the negative log-likelihood function, k denotes the number of parameters in the distribution function, and n denotes the sample size. The smallest AIC value represents the best fitting.

(2) Univariate return period

The univariate return period is calculated as follows (Shiau et al., 2001, 2006):

$$T_D = \frac{E_l}{1-F_D} \tag{7}$$

$$T_S = \frac{E_l}{1-F_S} \tag{8}$$

where E_l represents the expected inter-arrival time of drought events, and T_D and T_S represent the univariate return period of drought duration and severity, respectively.

The credible intervals (95%) based on the non-parametric bootstrap method (Kyselý et al., 2010) are used to quantify the sampling uncertainty. Specifically, the length between the upper boundary and lower boundary of the estimated drought duration (or drought severity) under a given return period is employed to evaluate the uncertainty of the univariate distribution:

$$L_{unc(\mathrm{D})}^{rp} = D_{up}^{rp} - D_{low}^{rp} \tag{9}$$

$$L_{unc(S)}^{rp} = S_{up}^{rp} - S_{low}^{rp} \tag{10}$$

where $L_{unc(\mathrm{D})}^{rp}$ and $L_{unc(S)}^{rp}$ are the measurements of sampling uncertainty for drought duration and severity in univariate frequency analysis, respectively, and S_{up}^{rp} (D_{up}^{rp}) and S_{low}^{rp} (D_{low}^{rp}) are the upper and lower boundaries of the drought severity (duration) under a given return period, respectively.

(3) Copula functions and Joint return period

The copula functions are employed to characterize the dependence structure of drought duration and severity. According to Sklar's theorem (Sklar, 1959), the bivariate probability distribution $F(d,s)$ can be expressed by its marginal distributions and the associated dependence function:

$$F(d,s) = C(F_D(d), F_S(s)) \tag{11}$$

where C denotes a copula function, and $F_D(d)$ and $F_S(s)$ denote the cumulative distribution functions of drought duration and severity, respectively.

In this study, the Gaussian, Gumbel and Frank copulas are identified as the candidate bivariate distributions (Nelsen, 2007):

$$C_{Gaussian}(\theta) = \Phi_\theta(\Phi^{-1}(F_D), \Phi^{-1}(F_S)) \qquad (\theta \in [-1,1]) \tag{12}$$

$$C_{Gumbel}(\theta) = \exp\{-[(-\ln(F_\mathrm{D})^\theta) + (-\ln(F_S)^\theta)]^{1/\theta}\} \qquad (\theta \in [1,\infty]) \tag{13}$$

$$C_{Frank}(\theta) = -\frac{1}{\theta}\ln[1+\frac{(e^{-\theta F_D}-1)(e^{-\theta F_S}-1)}{(e^{-\theta}-1)}] \quad (\theta \in [-\infty, \infty]). \tag{14}$$

The parameter Θ is estimated by the MLE method. The Akaike information criterion (AIC) is employed to evaluate the goodness-of-fit of the candidate copula functions.

The OR ($\{D \geq d\} \cup \{S \geq s\}$) and AND ($\{D \geq d\} \cap \{S \geq s\}$) cases are selected as the bivariate return periods in this study (Shiau et al., 2006; Zhang et al., 2015):

$$T_{or} = \frac{E_l}{1 - C(F_D, F_S)} \tag{15}$$

$$T_{and} = \frac{E_l}{1 - F_D - F_S + C(F_D, F_S)} \tag{16}$$

where T_{or} (T_{and}) denotes the OR (AND) return period, and $C(F_D, F_S)$ represents the combined cumulative distribution functions based on the copula functions.

(4) The most-likely scenario

For bivariate frameworks under a given T_{or} or T_{and}, there are infinite combinations of drought duration and severity which constitute a contour (or a design curve), albeit with different likelihoods of these combinations. In this study, the combination that has the largest probability to occur has been identified by utilizing the most-likely design realization method proposed by Salvadori et al. (2011). For a given joint return period T_{or}, the corresponding level $t = 1 - 1/T_{or}$ can easily be calculated, and the most-likely combination (MLC) point ($d*$, $s*$) of all possible events at this level can be obtained by selecting the point with the largest joint probability density (Salvadori et al. 2011):

$$(d*, s*) = \arg\max f(d, s) = c[F_D(d), F_S(s)]\, f_D(d)\, f_S(s) \tag{17}$$

$$C(F_D(\mathrm{d}), F_S(\mathrm{s})) = 1 - 1/T_{or} \tag{18}$$

where $f(d,s)$ represents the joint probability density function of drought duration and severity; $c[F_\mathrm{D}(\mathrm{d}), F_\mathrm{S}(\mathrm{s})] = dC(F_\mathrm{D}(\mathrm{d}), F_\mathrm{S}(\mathrm{s}))/d(F_\mathrm{D}(\mathrm{d}))d(F_S(\mathrm{s}))$ represents the density function of the copula; and $f_D(\mathrm{d})$ and $f_\mathrm{S}(\mathrm{s})$ are probability density functions of drought duration and severity, respectively. Since the analytical solutions are unavailable, the harmonic mean Newton's method is applied to estimate the results (Yin et al., 2018a, b).

(5) Bivariate uncertainty envelopes

To evaluate the uncertainty of the most-likely designs for droughts introduced by the limited sample size, the bootstrap method in the bivariate framework is used as follows:

a. Predefine the sample size *n* of bootstrapping samplings, and obtain the large sample *B* (b_1, b_2, $b_\mathrm{i,}$ …, b_n) involving *n* group of simulated drought duration and severity series (b_i).

b. For each sample series b_i in *B*, respectively use the simulated drought duration and severity to fit the marginal distributions and then select the most appropriate copula function.

c. For each sample b_i in *B* under a joint return period T_{or} or T_{and}, firstly estimate the most-likely design scenarios (d_i*, s_i*) by Eqs. (15)-(18) and then derive *n* pairs of most-likely design scenarios.

d. Under a joint return period T_{or} or T_{and}, use *n* pairs of most-likely design scenarios (d_i*, s_i*) calculated above to estimate a 95% confidence ellipse (Friendly et al., 2013). The area of the ellipse is used as the measurement of the sampling uncertainty under the bivariate framework.

3.4 Drought Hazard Propagation Ratio

(1) Drought hazard propagation ratio for most-likely designs

To further investigate the linkages between meteorological and hydrological drought hazards, a drought hazard propagation ratio for the most-likely design events (DHPR-MLE) is proposed. The DHPR-MLE is defined as the ratio between the meteorological and hydrological most-likely drought scenarios for a given return period:

$$DHPR-MLE^{RP} = \frac{MLE_h^{RP}}{MLE_m^{RP}} \quad (19)$$

where MLE_m^{RP} (MLE_h^{RP}) denotes the most-likely scenario of meteorological (hydrological) droughts for a given return period.

(2) Drought hazard propagation ratio for uncertainty envelopes

A drought hazard propagation ratio for the bivariate confidence envelope (DHPR-CE) is also proposed as a supplement of the design scenario. The DHPR-CE is defined as the ratio between the areas of the confidence ellipse for meteorological design scenarios and the areas of the confidence ellipse for hydrological design scenarios for a given return period:

$$DHPR-CE^{RP}=\frac{ER_h^{RP}}{ER_m^{RP}} \tag{20}$$

where ER_m^{RP} (ER_h^{RP}) denotes the bivariate confidence ellipse corresponding to the most-likely scenario of meteorological (hydrological) droughts for a given return period.

4 Results

4.1 Identification of Meteorological and Hydrological Drought Characteristics

Based on the theory of run, drought events were identified for the UYRB, the JSRB, and the JLRB, as shown in Figure 3. The upper three panels indicate meteorological droughts derived from the six-month SPEI, and the bottom three panels show hydrological droughts from the six-month SRI.

[Please insert Fig. 3 here]

Generally, the meteorological droughts tended to be more frequent than hydrological droughts for these catchments, with smaller severity and shorter duration. However, for events with long duration (>10 months), which might induce severe socio-economic losses, the hydrological droughts occur more frequently than the meteorological droughts. Additionally, notable meteorological droughts with the longest duration were not always consistent with notable hydrological droughts (See Table S1). This is because besides meteorological variables, other factors (e.g., antecedent soil moisture, groundwater recharge) might also play an important role in the formation of hydrological droughts.

To be specific, 63 meteorological and 35 hydrological drought events were recognized during the 1961–2014 period in the UYRB. The severe meteorological and hydrological droughts with long duration (>10 months) occurred 8 and 10 times, respectively. The longest meteorological drought duration spanned from June 1990 to February 1992 with a duration of 21 months (with a severity of 21.5), while the longest hydrological drought duration spanned from June 1969 to December 1971 with a duration of 31 months (with a severity of 24.2). The average duration and severity were 4.5 months and 4.97, respectively, for the 63 meteorological droughts, while they had almost increased by one time for hydrological droughts, with average duration of 7.5 months and average severity of 8.8.

In the JSRB, there were 9 meteorological droughts and 12 hydrological droughts with long duration (>10 months) during the 1961–2014 period. For meteorological droughts, there were 55 events in total. The average duration was 5.1 months and the average severity was 5.76. Moreover, the most severe event spanned 36 months from January 1971 to December 1973 (with a severity of 34.4). For hydrological droughts, 34 drought events were identified, with an average duration of 7.4 months and average severity of 8.76. Additionally, the longest event spanned 35 months from June 1975 to April 1978 (with a severity of 27.4).

In the JLRB, more notable meteorological droughts (12 times) with long duration were identified during 1961–2014 compared to notable hydrological droughts (9 times). Specifically, among 64 meteorological droughts, the longest spanned from January 2006 to June 2007 with 18 months in duration and 35.38 in severity, while among 55 hydrological droughts, the longest event spanned from August 1977 to January 1980 with 30 months in duration and 30.98 in severity. The average meteorological drought duration was 4.2 months with an average severity of 4.88, while the average hydrological drought duration was 4.6 months with an average severity of 5.29.

4.2 Propagation of Drought Characteristics

In order to better understand the overall pattern of drought events and intuitively reveal the relationship between meteorological and hydrological droughts, violin plots (Hintze et al., 1998) were used to investigate the distribution of drought duration and severity. The white circle in Figure 4 indicates the median of drought duration and severity from 1961 to 2014. The drought duration and severity derived from SPEI and SRI characterize "below-normal water availability" in the climatic (SPEI) and terrestrial (SRI) components of the hydrological cycle, respectively. Their dimensionless standardized property enables the comparison of drought duration and severity between meteorological episodes and hydrological episodes. Further, this comparison between the clusters in hydrological drought duration and severity and in meteorological drought duration and severity (characterized by the violin plots) facilitates to reveal the drought propagation processes that dominated by the synergetic impacts of local climates and catchment characteristics. (Van Loon et al., 2015; Yang et al., 2017; Liu et al., 2019). Generally, the distribution of the drought duration and severity between meteorological and hydrological events shows a similar pattern. All distributions are wide. They are even slightly wider for hydrological events than for meteorological events. These wide patterns imply great diversities across drought events. In addition, there are upward tendencies in terms of distributions of duration and severity from meteorological drought events to hydrological drought events across the three catchments, with larger changing amplitudes in the UYRB and JSRB than those in the JLRB. Again, these amplified drought signals denote deteriorated drought conditions from meteorological to hydrological propagation, which are consistent with previous studies (Yang et al., 2017; Liu et al., 2019).

[Please insert Fig. 4 here]

Furthermore, to probe into details how hydrological droughts response to meteorological droughts, we match some extreme hydrological droughts (with duration longer than 10 months) with corresponding meteorological droughts in Tables S2. The results show that there is the lagged response time from meteorological to hydrological droughts (for both the whole drought clusters and extreme episodes) over these 3 catchments. Generally speaking, these time-lags roughly range between 1 and 8 months over these three catchments. Specifically, the average time-lag in the JSRB was the longest (with an average time-lag of 4.1 months), followed by that in the JLRB (with an average time-lag of 1.7 months), and then in the UYRB (with an average time-lag of 1.1 months). Additionally, some negative time-lags emerged in the smaller watersheds (i.e., UYRB and JLRB), which might derive from the low antecedent soil moisture and limited groundwater storage capacity. Subsequently, a hydrological drought would occur in advance and it would even occur before a meteorological drought (Fleig et al., 2011; Liu et al., 2019).

4.3 Propagation of Univariate Drought Hazard

Prior to evaluating the bivariate hazard, it is essential to first perform drought analysis for marginal distributions. The candidate marginal distributions with the smallest AIC values for drought duration and severity were identified and are highlighted in bold in Table S3. The goodness-of-fit for duration and severity for the most appropriate distributions were further evaluated by the K–S test at the 0.05 significance level (Table S4). *H* values in Table S4 equaling to zero mean that the selected marginal distribution passes the K–S test and it is appropriate to be used. Also, the goodness-of-fit can be further demonstrated by *p*-values, with a larger *p*-value indicating a better fitting.

Figure 5 presents the fitted distribution and corresponding confidence intervals of duration and severity for meteorological and hydrological drought events over three catchments. Figure 6 shows the estimated design values and 95% confidence intervals for duration and severity under 10-, 20-, 30-, 50-, and 100-year return periods, respectively. In general, univariate design values under different return periods tend to increase from meteorological droughts to hydrological droughts in terms of both duration and severity. For instance, design values of the meteorological drought duration (severity) vary from 11.4 to 20.8 months (from 12.8 to 28.9) when return periods increase from 10 to 100 years in the UYRB, while those of the hydrological drought duration (severity) vary from 15.3 to 29.6 months (from 14.6 to 35.9). The increasing ratio in design values ranging from 14% to 42% clearly implies an increasing drought hazard in drought propagation processes.

In addition, the intervals of drought duration and severity are wide, particularly for high quantiles (or large return periods). Consistent with design values, the confidence intervals also noticeably ascend in drought propagation processes. Moreover, the increasing extent in the confidence intervals is even more remarkable than that in the design values (ranging from 67% to 100%). For example, the confidence intervals of the meteorological drought duration (severity) range from 15 to 24 months (from 18 to 35) for 10- and 100-year return periods for the UYRB, whereas those of the hydrological drought duration (severity) range from 30 to 49 months (from 30 to 60).

Similar results can be found in the JSRB and JLRB, which also demonstrate amplifying drought hazards under univariate frameworks in drought propagation processes.

[Please insert Figs. 5-6 here]

4.4 Propagation of Bivariate Drought Design

The correlations between drought duration and severity (as indicated by Pearson, Kendall, and Spearman coefficients), the goodness-of-fit (as denoted by AIC values), and parameters for the most preferred copulas are listed in Table S5. In general, drought duration and severity are highly correlated for these catchments. In addition, correlations between duration and severity in meteorological events are similar to those of hydrological events for all catchments, indicating that the dependence structure between drought characteristics may not be changed in the drought propagation process.

Figure 7 presents bivariate return periods of drought duration and severity under five different return periods (i.e. T=10-, 20-, 30-, 50- and 100-year), the most-likely design scenarios, and corresponding confidence envelopes for meteorological and hydrological droughts. The observations are also shown in the figure to obtain a rough estimation of their magnitudes in the bivariate context. As shown in the figure, most of the observed events are located below T_{or} = 50-year curve (T_{and} = 100-year curve) for these catchments. Generally, for any given bivariate drought event, the corresponding OR return period is larger than that of the AND, which indicates different design strategies. Additionally, for a given return period, the drought designs under the univariate framework are smaller than the most-likely design scenarios associated with the OR case, whereas they are larger than those associated with the AND case.

In general, from meteorological to hydrological droughts, there is an increasing tendency in the magnitude of the most-likely scenarios for both OR and AND cases.

This implies deteriorated hazards in drought propagation processes under the bivariate frameworks. For instance, for meteorological droughts in the UYRB, the most-likely designs are 10.5 (13.3) for severity and 9.8 (11.7) months for duration in the AND (OR) case under the 10-year return period, and 22.0 (32.3) for severity and 16.6 (22.5) months for duration in the AND (OR) case under the 100-year return period. In contrast, for hydrological droughts, the most-likely designs become 17.6 (19.3) for severity and 17.5 (18.5) months for duration under the 10-year return period, and 38.6 (40.9) for severity and 31.4 (32.9) months for duration under the 100-year return period. Increases in the magnitude of the most-likely scenarios from meteorological events to hydrological events are also found in the JSRB and JLRB.

Consistent with the magnitude of the most-likely scenarios, the uncertainty envelope of the OR case is also larger than that of the AND case. More importantly, an increasing tendency of the uncertainty envelopes can also be observed from meteorological to hydrological events in both OR and AND cases. These increasing amplitudes are even more pronounced with return periods ascending. For example, in the UYRB, the area of the uncertainty envelope is 20.6 (17.0) for meteorological events in the AND (OR) case under the 10-year return period, whereas it is almost doubled for hydrological events, with the uncertainty envelope area being equal to 40.6 (53.1). Under the 100-year return period, the area of the uncertainty envelope is 80.9 (96.4) for meteorological events in the AND (OR) case, while it is roughly 3 times larger for hydrological events, with the uncertainty envelope area being equal to

204.7 (236.2) in the AND (OR) case. As expected, similar results can also be observed in the JLRB and JSRB.

[Please insert Fig. 7 here]

4.5 Propagation of Drought Hazard Analysis

The return levels ranging between 10- to 200-year for drought duration and severity, as well as the most-likely scenarios for meteorological and hydrological events over the three catchments are displayed in Figure 8. As expected, magnitudes of both meteorological and hydrological drought designs increase gradually with return periods ascending.

To further investigate changes of hazards in drought propagation with return periods ascending, the drought hazard propagation ratio (DHPR) calculated by Equations (19) and (20) are shown in Figure 9 for the three catchments. The upper three panels show the DHPR for the most-likely scenarios in the AND and OR cases, whereas the bottom three panels demonstrate the DHPR for the corresponding confidence ellipse. The results show that with return periods ascending, the DHPR shows slight fluctuations for the most-likely scenarios and their corresponding uncertainty ellipse.

Specifically, the DHPR consistently ranges between 1 and 2 for the most-likely scenarios in the AND and OR cases over these catchments. Nevertheless, the DHPR-MLE in the larger catchment (JSRB) tends to be more stable than that in the smaller catchments (i.e., UYRB, JLRB) for duration and severity in both AND and

OR cases.

The DHPR for confidence ellipse is roughly higher than that for the most-likely scenarios. Specifically, the DHPR for confidence ellipse in both AND and OR cases ranges between 2 and 3 over the three catchments, which demonstrates the stability of hazard transferability from meteorological to hydrological droughts.

[Please insert Figs. 8-9 here]

4.6 Generalization of the proposed framework

To confirm the stability of drought hazard propagation ratio for both the most likely scenario and the corresponding confidence ellipse, this framework is extended to test over 218 small-scale catchments in the United States. The best-performed marginal distributions and appropriate Copula types are presented in Figure. S1. As shown, the selected marginal distributions and Copula types for the meteorological droughts are similar to those for the hydrological droughts to some extent. This indicates the close relationships between these two drought categories. The 20-, 50-, 100-year most likely scenarios (under the OR case) of severity and duration for meteorological (and hydrological) droughts are demonstrated in Figures S2-S3, respectively. As expected, for a given return period, the severity and duration of hydrological droughts are prone to be larger than those of meteorological droughts. For instance, under the 20-year joint return period, the most likely scenarios of severity are below 20 for meteorological droughts over those catchments, while they roughly range between 20 and 40 for hydrological droughts. This phenomenon also holds for the corresponding confidence ellipse (Figure. S4). Figures 10-11 present the DHPR-MLE for drought severity and duration, respectively. It can be observed that the DHPR-MLE almost stay unchanged for both drought duration and severity with the joint return period increasing over the 218 catchments. In addition, the DHPR-MLE in most catchments are higher than 1. This implies the lengthening and exacerbating phenomenon in drought propagation from the meteorological circumstance to the underlying surfaces. Furthermore, the DHPR-CE is presented in Figure 12 for those catchments. Similar to the pattern of DHPR-MLE, the DHPR-CE typically remains the same with the joint return period ascending, though larger spatial variations are observed. Overall, those results confirm the stability of DHPR.

[Please insert Figs. 10-12 here]

5 Discussion

It is well known that a hydrological drought usually stems from a meteorological drought and is determined by the propagation of meteorological drought through the terrestrial hydrological cycle (Van Loon et al., 2015). To investigate the climate conditions inducing a hydrological drought, we identify the SPEI-6 value at the onset of a hydrological drought and accumulate negative SPEI-6 values forward until it becomes above zero. To further elaborate the correlations between these two types of droughts, the drought duration and severity derived from SPEI-6 with the corresponding hydrological drought is compared. The notorious drought episodes longer than 10 months (listed in Table S2) are selected and are employed to demonstrate the corresponding results for the three catchments in Tables S6. It can be observed that when a hydrological drought occurs, the current-month SPEI-6 value is generally lower than the SRI-6 value and the antecedent cumulative SPEI-6 value is even much lower than the SRI-6. This verifies that abnormally dry climates can induce a hydrological drought. Furthermore, it can be observed that during a hydrological drought with long persistent time and large severity, the dry duration and magnitude characterized by SPEI-6 are also considerable, but smaller than the corresponding values calculated by SRI-6. For instance, in the UYRB, the hydrological drought occurred between June, 1969 and December, 1971 which lasted 31 months with a severity of 35.72, the corresponding dry months are 25 months with a magnitude of 29.30. This indicates that the exacerbated conditions in drought propagation processes (Van Loon et al., 2014). In short, hydrological droughts are generally related to abnormally dry climates and sustained “below-normal water availability” in climates which typically contribute to large magnitudes of hydrological droughts.

To further probe into the drought propagation regimes of these three catchments that spans from humid to semi-arid climates and involves different catchment characteristics, the correlations between SPEI and SRI are connected with local rainfall-runoff relationships. The results show that the correlation between SPEI and SRI is highly dependent on the relationship between precipitation and runoff. Variations of other recharge (e.g., snowmelt, groundwater discharge) to runoff cannot be captured by SPEI and may weaken this correlation. Therefore, in the UYRB (with the rainfall–runoff coefficient being 0.31) the correlation between SPEI and SRI is weaker than that in the JSRB and JLRB (with the rainfall–runoff coefficients being 0.48 and 0.51, respectively). Additionally, though the time-delay phenomenon in drought propagation processes can be observed, the time-lags differ among the three catchments. For instance, the longest time-lag between hydrological and meteorological droughts emerges in the JSRB. This may be due to the fact that the widely distributed coniferous forests, hard-wood forest and bush-wood in this catchment, and the large drainage area contribute to the prolonging of hydrological responses to the abnormally dry climates (Donohue et al., 2011; Ye et al., 2015; Liu et al., 2016).

The notion of "return period" (or "design quantile") that is closely related to the concept of "hazard" is frequently used in practice for the identification of dangerous events. In the multivariate framework, a given return period usually means infinite combinations for each variable involved and thus additional information is needed to pick out a single scenario in practice. Traditionally, for a given return period, the design scenario with the same marginal distribution probability for each variable has been identified and used (Zscheischler et al., 2017). However, this scenario deriving from the same probability for each variable is neither the most conservative estimation, nor the most-likely scenario to happen, lacking statistical consideration and physical mechanism. Consequently, the most-likely realization (Salvadori et al., 2011; Yin et al., 2018b) under the multivariate case is employed in this study. This design represents a scenario that is "more likely" to happen than others. Furthermore, the effectiveness and safety of design strategies for this scenario has been validated and can be the reasonable candidate in multivariate hazard assessments. Also, the uncertainty correlated with the most-likely design that has raised lots of attentions in the univariate context is usually ignored in the multivariate cases. This study quantifies such bivariate uncertainty and investigates the propagation process from meteorological conditions to hydrological responses. The results show that the magnitudes of the most-likely scenarios are inclined to increase from meteorological to hydrological droughts. At the same time, the corresponding uncertainty envelopes that are measured by the confidence ellipses also tend to ascend in drought propagation. This clearly implies deteriorated hazards of hydrological responses to abnormal climatic dryness. Moreover, it is worth noting that the DHPR for both the most-likely scenarios and corresponding bivariate uncertainty are relatively stable under different return periods. This may reveal the steady correlations between meteorological drought hazards and hydrological drought hazards.

On the other hand, since drought severity are accumulated values of SPEI or SRI that below zero during the drought events, the values of severity thus includes variations of drought duration to some extent. To tackle this problem and verify the robustness of our results that the proposed DHPR-MLE and DHPR-CE are stable in drought propagation, the intensity is employed to characterize droughts to serve as a comparison. This intensity is obtained by dividing the original “severity” by the “duration”, which can thus avoid the effect of drought duration. The newly calculated drought propagation ratio following the proposed framework is investigated (Figures. 13-14). The results show that the DHPR-MLE (of duration and intensity) and DHPR-CE remain stable. Distinct from the DHPR-MLE of drought severity, the DHPR-MLE of drought intensity is no longer higher than 1 in the UYRB. This demonstrates that the enlarged severity from the meteorological droughts to the hydrological droughts in the UYRB is mainly caused by lengthened durations, while in the JSRB and JLRB, it is more related to strengthened intensities, which implies the differences of local climates and catchment characteristics across the three catchments. Overall, the above indicates that DHPR-MLE (of severity and duration) and DHPR-CE are stable and our conclusions are robust.

[Please insert Figs. 13-14 here]

The proposed framework provides a unique perspective to systematically understand the drought propagation process, especially for the variation of drought hazards. However, there are also some limitations in this study. For instance, to reduce sampling uncertainty, the value of zero is employed as the threshold to identify droughts for including minor to moderate drought events. Further studies may use different threshold values to explore their contributions to drought hazard transferability. In addition, some previous studies (Barker et al., 2016; Yang et al., 2017) have indicated that the climatic properties, catchment landscape, and groundwater conditions all play an important role in drought propagation. Future studies may explore and even quantify their relative contributions regarding hazard variations in drought propagation. Another issue that should be noted is that this study only investigated the hazard transferability, while did not quantify the drought risk due to paucity of data. The investigation of risk variation in drought propagation by further incorporating the exposure (e.g., population) and vulnerability (e.g., land use, economy, health, energy, and infrastructure) components (Ahmadalipour et al., 2018, 2019) may also be an avenue for future studies.

6 Conclusions

Understanding drought propagation is essential to developing efficient drought adaptation policies and drought management plans. This study proposed a framework with incorporation of copulas and the DHPR to examine hazard transferability from meteorological to hydrological droughts. The proposed framework was applied to three different basins in China and further tested over 218 small-scale catchments in the United States.

Generally, there is a lagging effect for meteorological to hydrological drought propagations. The longest time-lag emerges in the JSRB. Time-lags in the JLRB and UYRB are shorter, with average values both smaller than 2 months. The duration and severity of meteorological droughts are both amplified when propagating to hydrological droughts among the three catchments, reflecting a deteriorated condition in drought propagation. Drought hazards denoted by the most-likely scenarios and corresponding bivariate confidence ellipses from climatic “below-normal water availability” to the terrestrial hydrological part pronouncedly ascend across all the 3 catchments, as well as over the tested 218 catchments. It also can be found that the hazard transferability processes are relatively stable, as indicated by the almost unchanged DHPR-MLE and DHPR-CE with return periods increasing. To be specific, the DHPR-MLE tends to be smaller than the DHPR-CE.

In summary, this study shows that there is a strong and stable linkage between meteorological and hydrological drought hazards and this linkage can be reflected in unchanged DHPR-MLE and DHPR-CE. Results of this study can provide useful information to understand the drought propagation mechanisms in hydrological systems.

Acknowledgments

This work was partially supported by the National Key Research and Development Program of China (No. 2017YFA0603704), the National Natural Science Foundation of China (Grant Nos. 51779176, 51811540407), the Overseas Expertise Introduction Project for Discipline Innovation (111 Project) funded by Ministry of Education and State Administration of Foreign Experts Affairs P.R. China (Grant No. B18037), and the Thousand Youth Talents Plan from the Organization Department of CCP Central Committee (Wuhan University, China). The authors wish to thank the China Meteorological Data Sharing Service System for providing gauged meteorological data, the Yangtze River Water Resources Commission and the Yellow River Water Resources Commission in China for providing runoff records.

Conflict of interest

The authors declare that they have no conflict of interest with the work presented here.

7 References

Ahmad, M. I., Sinclair, C. D., & Werritty, A. (1988). Log-logistic flood frequency analysis. Journal of Hydrology, 98(3-4), 205-224.

Ahmadalipour, A., Moradkhani, H., & Demirel, M. C. (2017). A comparative assessment of projected meteorological and hydrological droughts: elucidating the role of temperature. Journal of hydrology, 553, 785-797.

Ahmadalipour, A., & Moradkhani, H. (2018). Multi-dimensional assessment of drought vulnerability in Africa: 1960–2100. Science of the total environment, 644, 520-535.

Ahmadalipour, A., Moradkhani, H., Castelletti, A., & Magliocca, N. (2019). Future drought risk in Africa: Integrating vulnerability, climate change, and population growth. Science of the Total Environment, 662, 672-686.

Allen, R. G., Pereira, L. S., Raes, D., & Smith, M. (1998). Crop evapotranspiration-Guidelines for computing crop water requirements-FAO Irrigation and drainage paper 56. Fao, Rome, 300(9), D05109.

Ayantobo, O. O., Li, Y., Song, S., & Yao, N. (2017). Spatial comparability of drought characteristics and related return periods in mainland China over 1961–2013. Journal of hydrology, 550, 549-567.

Ayantobo, O. O., Li, Y., Song, S., Javed, T., & Yao, N. (2018). Probabilistic modelling of drought events in China via 2-dimensional joint copula. Journal of hydrology, 559, 373-391.

Apurv, T., Sivapalan, M., & Cai, X. (2017). Understanding the role of climate characteristics in drought propagation. Water Resources Research, 53(11), 9304-9329.

Bozdogan, H. (1987). Model selection and Akaike's information criterion (AIC): The general theory and its analytical extensions. Psychometrika, 52(3), 345-370.

Barker, L. J., Hannaford, J., Chiverton, A., & Svensson, C. (2016). From meteorological to hydrological drought using standardized indicators. Hydrology and Earth System Sciences, 20(6), 2483-2505.

Chang, J., Li, Y., Wang, Y., & Yuan, M. (2016). Copula-based drought risk assessment combined with an integrated index in the Wei River Basin, China. Journal of Hydrology, 540, 824-834.

Cancelliere, A., & Salas, J. D. (2010). Drought probabilities and return period for annual streamflow’s series. Journal of Hydrology, 391(1-2), 77-89.

Cuo, L., Zhang, Y., Gao, Y., Hao, Z., & Cairang, L. (2013). The impacts of climate change and land cover/use transition on the hydrology in the upper Yellow River basin, China. Journal of Hydrology, 502, 37-52.

Dai M, Huang SZ*, Huang Q, et al., 2020. Assessing agricultural drought risk and its dynamic evolution characteristics. Agricultural Water Management, 231, 106003.

Donohue, R. J., M. L. Roderick, and T. R. McVicar (2011), Assessing the differences in sensitivity of runoff to changes in climatic conditions across a large basin, J. Hydrol., 406(3), 234–244, doi:10.1016/j.jhydrol.2011.07.003

Farnsworth, R. K., & Thompson, E. S. (1982). Mean monthly, seasonal, and annual pan evaporation for the United States (pp. 23-25). National Oceanic and Atmospheric Administration, National Weather Service.

Fay M P, Feuer E J. Confidence intervals for directly standardized rates: a method based on the gamma distribution [J]. Statistics in medicine, 1997, 16(7): 791-801.

Fleig, A. K., Tallaksen, L. M., Hisdal, H., and Hannah, D. M.: Regional hydrological drought in north-western Europe: linking a new regional drought area index with weather types, Hydrol. Process., 25, 1163–1179, 2011.

Friendly M, Monette G, Fox J. Elliptical insights: understanding statistical methods through elliptical geometry[J]. Statistical Science, 2013, 28(1): 1-39.

Folland, C. K., Hannaford, J., Bloomfield, J. P., Kendon, M., Svensson, C., Marchant, B. P., ... & Wallace, E. (2015). Multi-annual droughts in the English Lowlands: a review of their characteristics and climate drivers in the winter half-year. Hydrology and Earth System Sciences, 19(5), 2353-2375.

Gu, L., Chen, J., Xu, C. Y., Wang, H. M., & Zhang, L. (2018). Synthetic impacts of internal climate variability and anthropogenic change on future meteorological droughts over China. Water, 10(11), 1702.

Gu, L., Chen, J., Xu, C. Y., Kim, J. S., Chen, H., Xia, J., & Zhang, L. (2019). The contribution of internal climate variability to climate change impacts on droughts. Science of The Total Environment, 684, 229-246.

Gu, L., Chen, J., Yin, J., Sullivan, S. C., Hui-Min, W., Guo, S., ... & Jong-Suk, K. (2020). Projected increases in magnitude and socioeconomic exposure of global droughts in 1.5 and 2° C warmer climates. Hydrology and Earth System Sciences, 24(1), 451-472.

Guo Y., Huang S.*, Huang Q., Leng G., Fang W., Wang L., Wang H., 2020.

Propagation thresholds of meteorological drought for triggering hydrological drought at various levels. Sci. Total Environ., 712, 136502.

Hintze, J. L., & Nelson, R. D. (1998). Violin plots: a box plot-density trace synergism. The American Statistician, 52(2), 181-184.

Hao, Z., & Singh, V. P. (2015). Drought characterization from a multivariate perspective: A review. Journal of Hydrology, 527, 668-678.

Haslinger, K., Koffler, D., Schöner, W., & Laaha, G. (2014). Exploring the link between meteorological drought and streamflow: Effects of climate‐catchment interaction. Water Resources Research, 50(3), 2468-2487.

Hayes, M., M. Svoboda, N. Wall, and M. Widhalm, 2011: The Lincoln declaration on drought indices: Universal meteorological drought index recommended. Bull. Amer. Meteor. Soc., 92, 485–488.

Huang, S., Huang, Q., Chang, J., & Leng, G. (2016). Linkages between hydrological drought, climate indices and human activities: a case study in the Columbia River basin. International Journal of climatology, 36(1), 280-290.

Huang, S., Li, P., Huang, Q., Leng, G., Hou, B., & Ma, L. (2017). The propagation from meteorological to hydrological drought and its potential influence factors. Journal of hydrology, 547, 184-195.

Jiang, C., Xiong, L., Yan, L., Dong, J., & Xu, C. Y. (2019). Multivariate hydrologic design methods under nonstationary conditions and application to engineering practice. Hydrology and Earth System Sciences, 23(3), 1683-1704.

Kyselý, J. (2010). Coverage probability of bootstrap confidence intervals in heavy-tailed frequency models, with application to precipitation data. Theoretical and Applied Climatology, 101(3-4), 345-361.

Kwon, H. H., & Lall, U. (2016). A copula‐based nonstationary frequency analysis for the 2012‑2015 drought in California. Water Resources Research, 52(7), 5662-5675.

Liu, Q., T. R. McVicar, Z. F. Yang, R. J. Donohue, L. Q. Liang, and Y. T. Yang (2016), The hydrological effects of varying vegetation characteristics in a temperate water-limited basin: Development of the dynamic Budyko-Choudhury-Porporato (dBCP) model, J. Hydrol., 543, 595– 611, doi:10.1016/j.jhydrol.2016.10.035

Liu, Y., Zhu, Y., Ren, L., Singh, V. P., Yong, B., Jiang, S., ... & Yang, X. (2019). Understanding the spatiotemporal links between meteorological and hydrological droughts from a three-dimensional perspective. Journal of Geophysical Research: Atmospheres, 124(6), 3090-3109.

Lorenzo-Lacruz, J., Vicente-Serrano, S. M., González-Hidalgo, J. C., López-Moreno, J. I., & Cortesi, N. (2013). Hydrological drought response to meteorological drought in the Iberian Peninsula. Climate Research, 58(2), 117-131.

MWR (Ministry of Water Resources) (2006) Regulations for calculating design flood of water resources and hydropower projects. Water Resources and Hydropower Press, Beijing (in Chinese)

Mishra, A. K., & Singh, V. P. (2010). A review of drought concepts. Journal of hydrology, 391(1-2), 202-216.

Medved-Cvikl, B., Ceglar, A., Kajfe-Bogataj, L., 2012. The response of hydrological droughts to climatic droughts at different time scales in Dravinja, Savinja and Krka basins in Slovenia. Ohrid, Republic of Macedonia, BALWOIS.

Nelsen, R. B. (2007). An introduction to copulas. Springer Science & Business Media.

Salvadori, G., Michele, C. D., & Durante, F. (2011). On the return period and design in a multivariate framework. Hydrology and Earth System Sciences, 15(11), 3293-3305.

Shiau, J.T., Shen, H.W., 2001. Recurrence analysis of hydrologic droughts of differing severity. J. Water Resour. Plann. Manage. 127 (1), 30–40.

Shiau, J. T., Wang, H. Y., & Tsai, C. T. (2006). Bivariate frequency analysis of floods using copulas1. Journal of the American Water Resources Association, 42(6), 1549-1564.

Sklar, M.: Fonctions de Répartition a n Dimensions et Leurs Marges, 8 pp., Univ. Paris, Paris, 1959.

Shukla, S., & Wood, A. W. (2008). Use of a standardized runoff index for characterizing hydrologic drought. Geophysical research letters, 35(2).

Su, B., Huang, J., Fischer, T., Wang, Y., Kundzewicz, Z. W., Zhai, J., ... & Tao, H. (2018). Drought losses in China might double between the 1.5 C and 2.0 C warming. Proceedings of the National Academy of Sciences, 115(42), 10600-10605.

Van Loon, A. F., Tijdeman, E., Wanders, N., Van Lanen, H. J., Teuling, A. J., & Uijlenhoet, R. (2014). How climate seasonality modifies drought duration and deficit. Journal of Geophysical Research: Atmospheres, 119(8), 4640-4656.

Van Loon, A. F., & Laaha, G. (2015). Hydrological drought severity explained by climate and catchment characteristics. Journal of hydrology, 526, 3-14.

Vidal, J. P., Martin, E., Franchistéguy, L., Habets, F., Soubeyroux, J. M., Blanchard, M., & Baillon, M. (2010). Multilevel and multiscale drought reanalysis over France with the Safran-Isba-Modcou hydrometeorological suite. Hydrology and Earth System Sciences Discussions, 14(3), 459-478.

Vicente-Serrano, S. M., & López-Moreno, J. I. (2005). Hydrological response to different time scales of climatological drought: an evaluation of the Standardized Precipitation Index in a mountainous Mediterranean basin.

Vicente-Serrano, S.M., Beguería, S., López-Moreno, J.I., 2010. A multiscale drought index sensitive to global warming: the standardized precipitation evapotranspiration index. J Climate, 23(7): 1696-1718. DOI:10.1175/2009jcli2909.1

Vicente-Serrano, S. M., Beguería, S., Lorenzo-Lacruz, J., Camarero, J. J., López-Moreno, J. I., Azorin-Molina, C., ... & Sanchez-Lorenzo, A. (2012). Performance of drought indices for ecological, agricultural, and hydrological applications. Earth Interactions, 16(10), 1-27.

Wang, D., & Hejazi, M. (2011). Quantifying the relative contribution of the climate and direct human impacts on mean annual streamflow in the contiguous United States. Water Resources Research, 47(10).

Wang, W., Ertsen, M. W., Svoboda, M. D., & Hafeez, M. (2016). Propagation of drought: from meteorological drought to agricultural and hydrological drought. Advances in Meteorology, 2016.

Weng, B., Zhang, P., & Li, S. (2015). Drought risk assessment in China with different spatial scales. Arabian Journal of Geosciences, 8(12), 10193-10202.

Wong, G., Van Lanen, H. A. J., & Torfs, P. J. J. F. (2013). Probabilistic analysis of hydrological drought characteristics using meteorological drought. Hydrological Sciences Journal, 58(2), 253-270.

Yang, Y., McVicar, T. R., Donohue, R. J., Zhang, Y., Roderick, M. L., Chiew, F. H. S., & Zhang, J. (2017). Lags in hydrologic recovery fol-lowing an extreme drought: Assessing the roles of climate and catchment characteristics. Water Resources Research, 53, 4821–4837. https://doi.org/10.1002/2017WR020683

Ye, S., H. Li, S. Li, L. Leung, Y. Demissie, and Q. Ran (2015), Vegetation regulation on streamflow intra-annual variability through adaption to climate variations.

Geophys. Res. Lett., 42, 10,307–10,315, doi:10.1002/2015GL066396.

Yevjevich, V. M. (1967). Objective approach to definitions and investigations of continental hydrologic droughts, An. Hydrology papers (Colorado State University); no. 23.

Yin, J., Guo, S., Liu, Z., Yang, G., Zhong, Y., & Liu, D. (2018a). Uncertainty analysis of bivariate design flood estimation and its impacts on reservoir routing. Water resources management, 32(5), 1795-1809.

Yin, J., Guo, S., He, S., Guo, J., Hong, X., & Liu, Z. (2018b). A copula-based analysis of projected climate changes to bivariate flood quantiles. Journal of hydrology, 566, 23-42.

Yin, J., Guo, S., Wu, X., Yang, G., Xiong, F., & Zhou, Y. (2019). A meta-heuristic approach for multivariate design flood quantile estimation incorporating historical information. Hydrology Research, 50(2), 526-544.

Zargar, A., Sadiq, R., Naser, B., & Khan, F. I. (2011). A review of drought indices. Environmental Reviews, 19(NA), 333-349.

Zhai, J., Su, B., Krysanova, V., Vetter, T., Gao, C., & Jiang, T. (2010). Spatial variation and trends in PDSI and SPI indices and their relation to streamflow in 10 large regions of China. Journal of Climate, 23(3), 649-663.

Zhang, Q., Qi, T., Singh, V. P., Chen, Y. D., & Xiao, M. (2015). Regional frequency analysis of droughts in China: a multivariate perspective. Water Resources Management, 29(6), 1767-1787.

Zhang, D., Chen, P., Zhang, Q., & Li, X. (2017). Copula-based probability of concurrent hydrological drought in the Poyang lake-catchment-river system (China) from 1960 to 2013. Journal of hydrology, 553, 773-784.

Zhu, Y., Wang, W., Singh, V. P., & Liu, Y. (2016). Combined use of meteorological drought indices at multi-time scales for improving hydrological drought detection. Science of the Total Environment, 571, 1058-1068.

Zscheischler, J., & Seneviratne, S. I. (2017). Dependence of drivers affects risks associated with compound events. Science Advances, 3(6), e1700263.

Figures

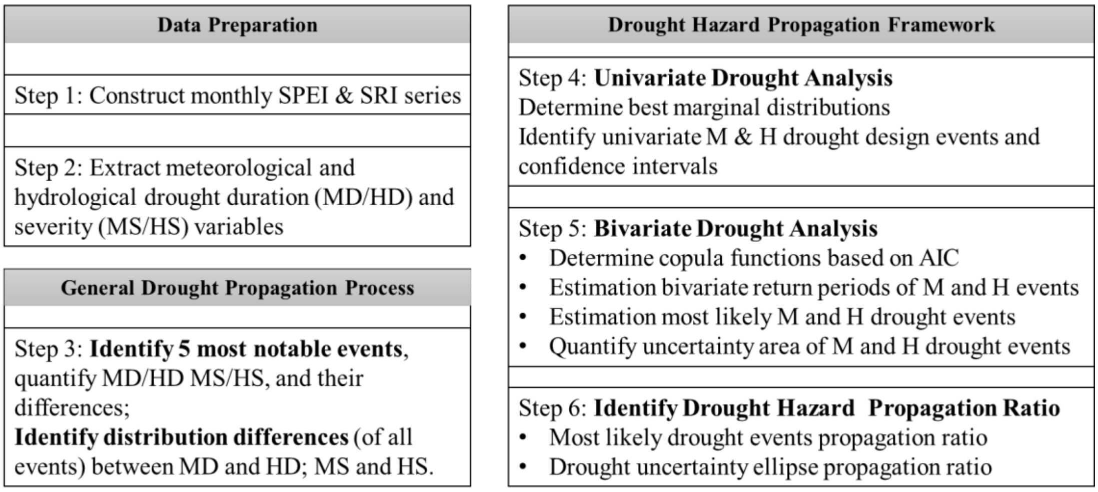

Figure 1 A schematic framework of the drought hazard propagation analysis.

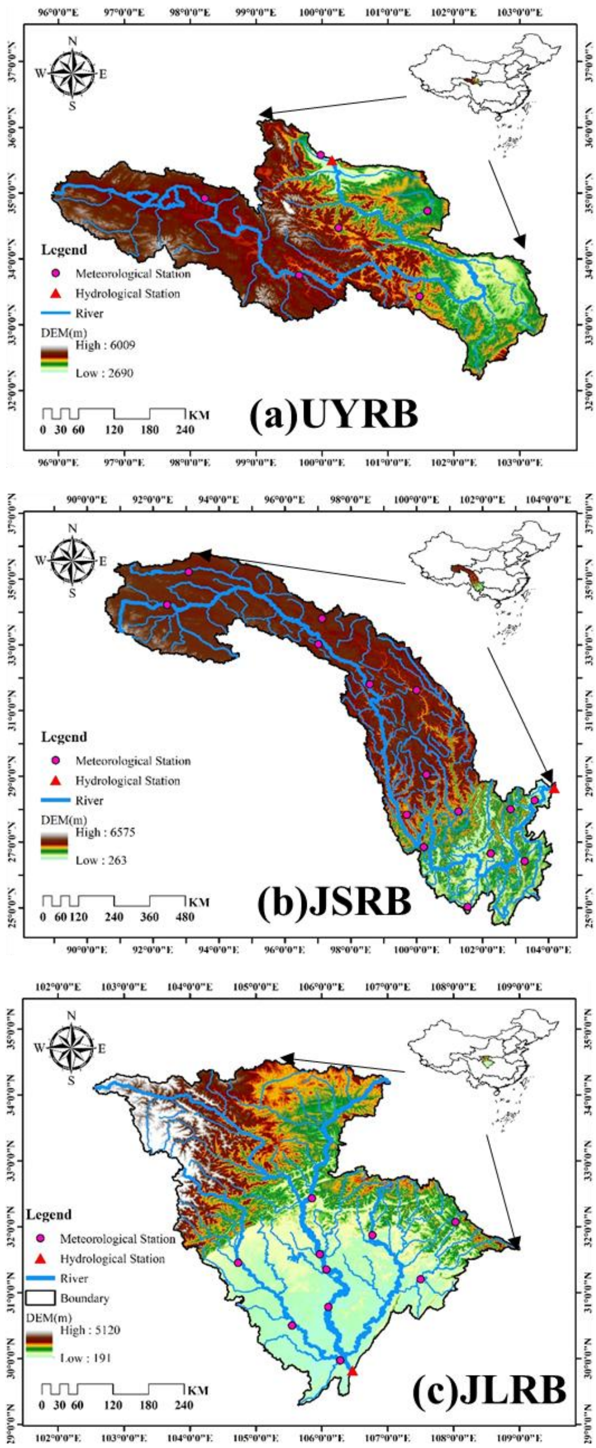

Figure 2 Location of three catchments used in this study and corresponding hydrological and meteorological stations: (a) UYRB, the upper Yellow River basin controlled by the Tang-Naihai Station; (b) JSRB, the Jinsha River basin located in the upper Yangtze River basin and controlled by the Ping-Shan Station; (c) JLRB, the Jialing River basin located in the middle Yangtze River basin and controlled by the Bei-Pei Station.

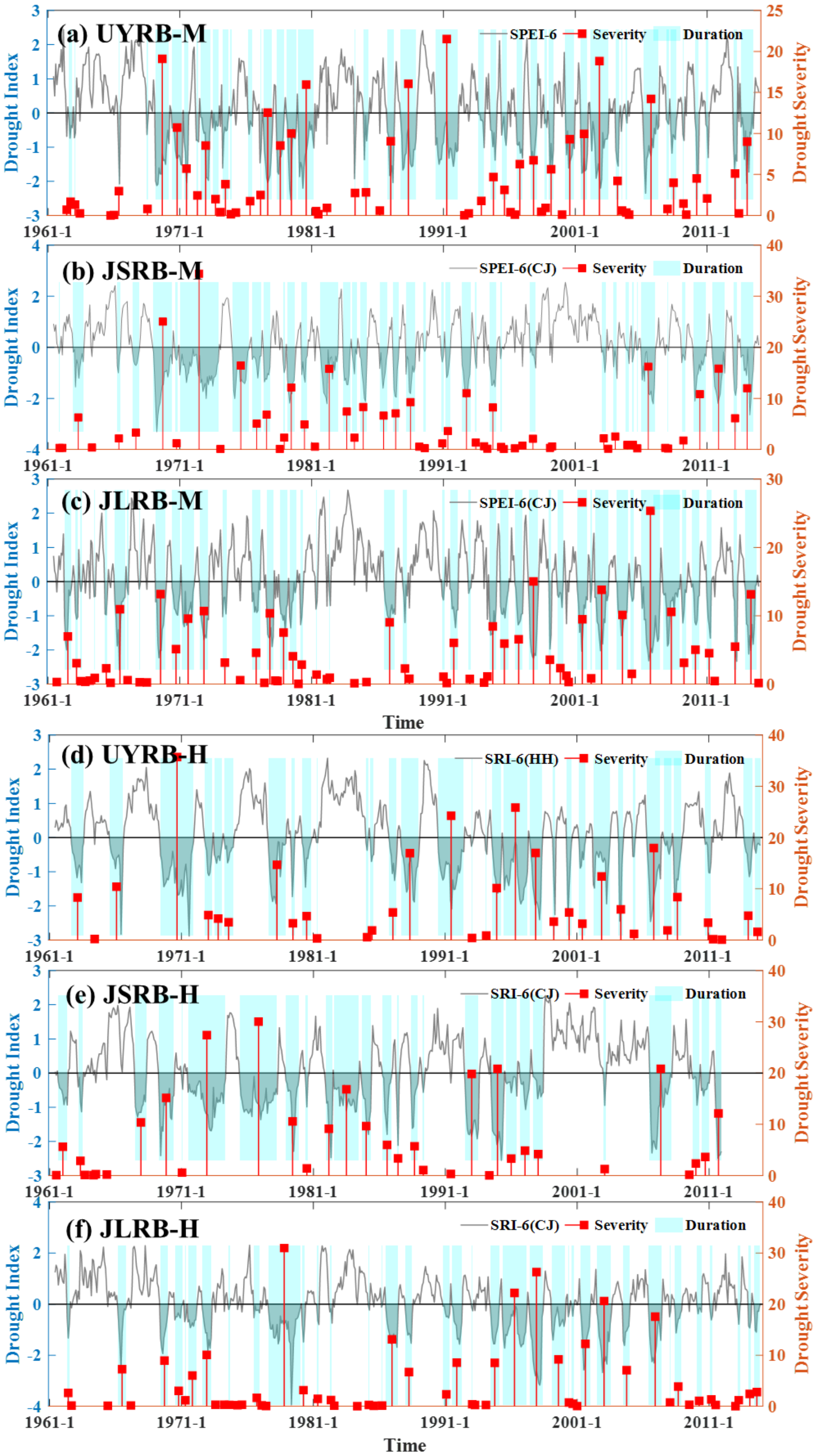

Figure 3 Time series of SPEI-6 and SRI-6 and corresponding meteorological drought (M) and hydrological drought (H) duration and severity.

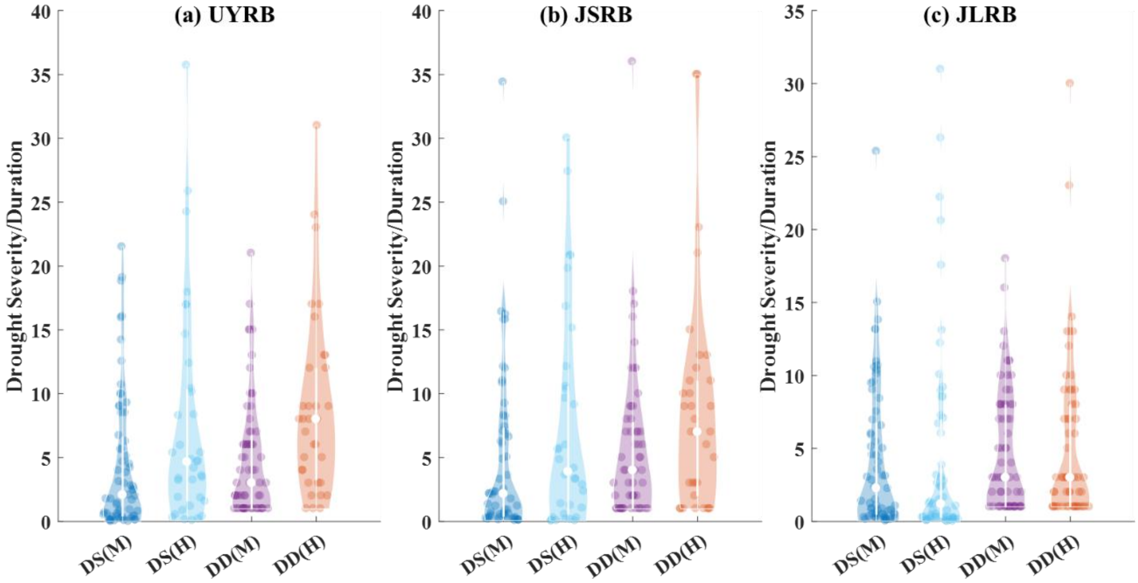

Figure 4 Violin plot of the meteorological drought severity (DS(M)) and drought duration (DD(M)), and the hydrological drought severity (DS(H)) and drought duration (DD(H)).

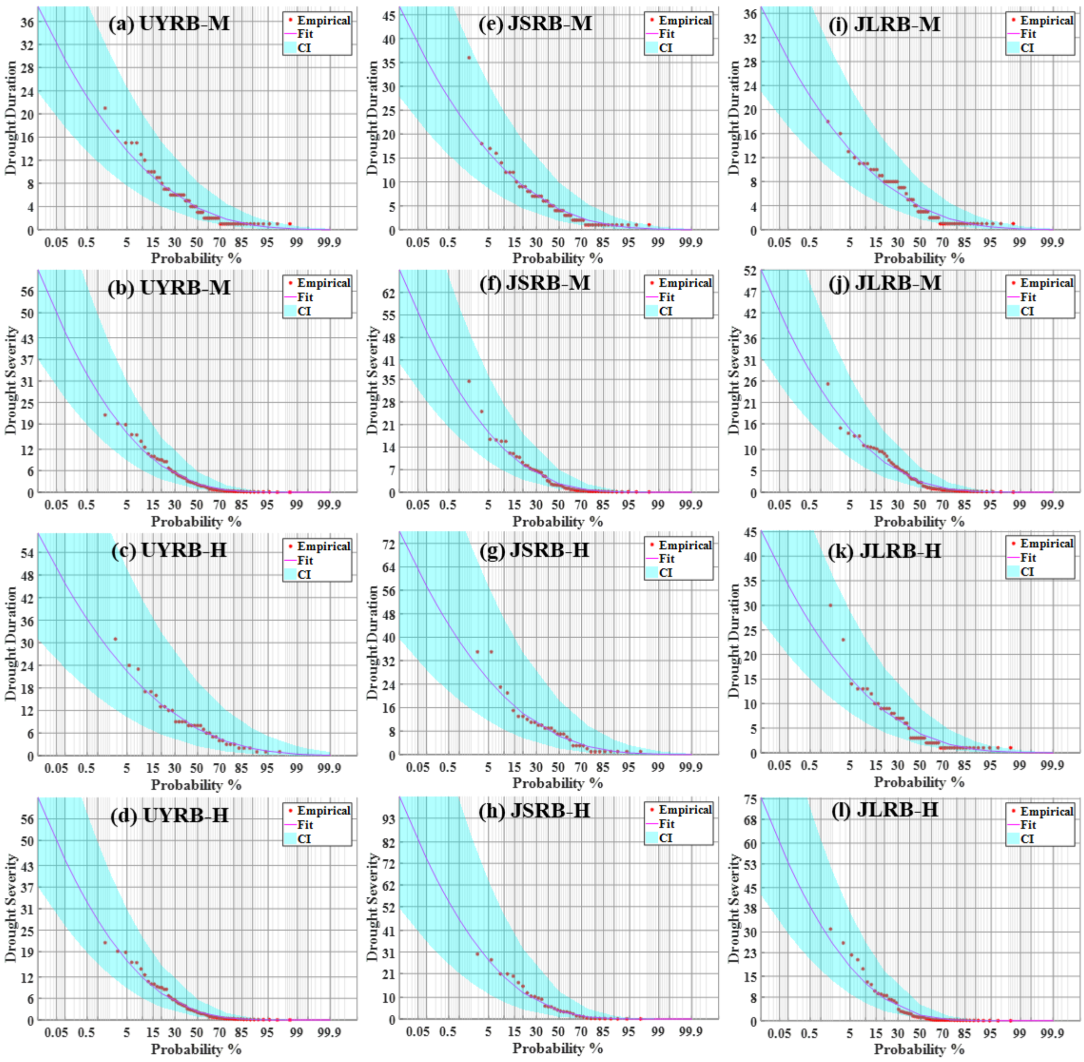

Figure 5 Univariate frequency analysis for the meteorological droughts (M) and the hydrological droughts (H) in the three catchments. The red dots denote the empirical distributions; the magenta lines denote the best fitted distributions; the cyan regions denote the 95% confidence intervals.

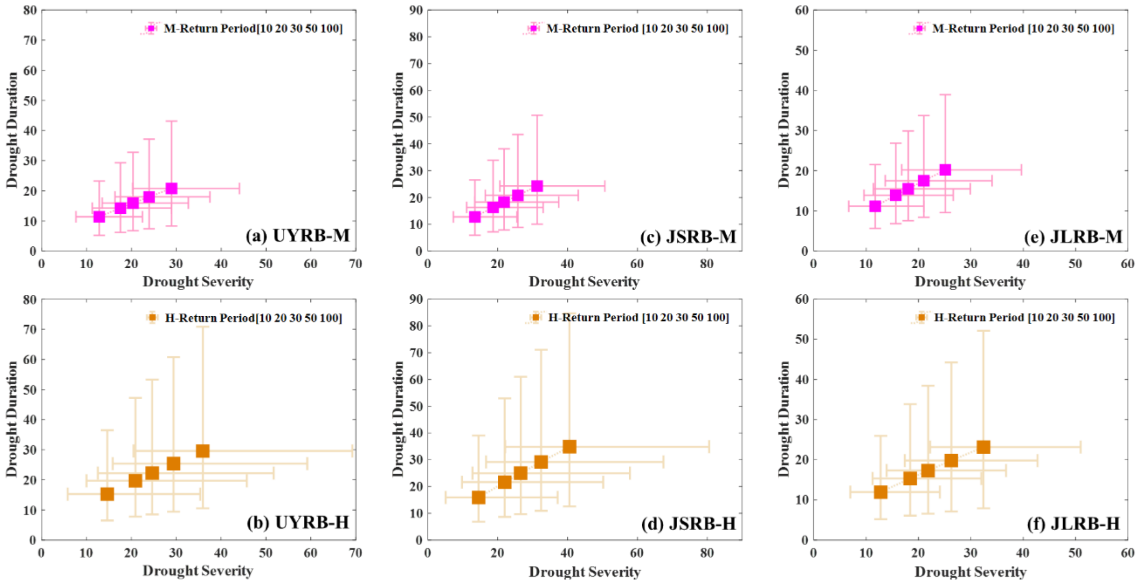

Figure 6 Univariate design values and interval widths of 95% confidence intervals for meteorological droughts (M) and hydrological droughts (H) under 10-, 20-, 30-, 50-, and 100-year return periods for the three catchments.

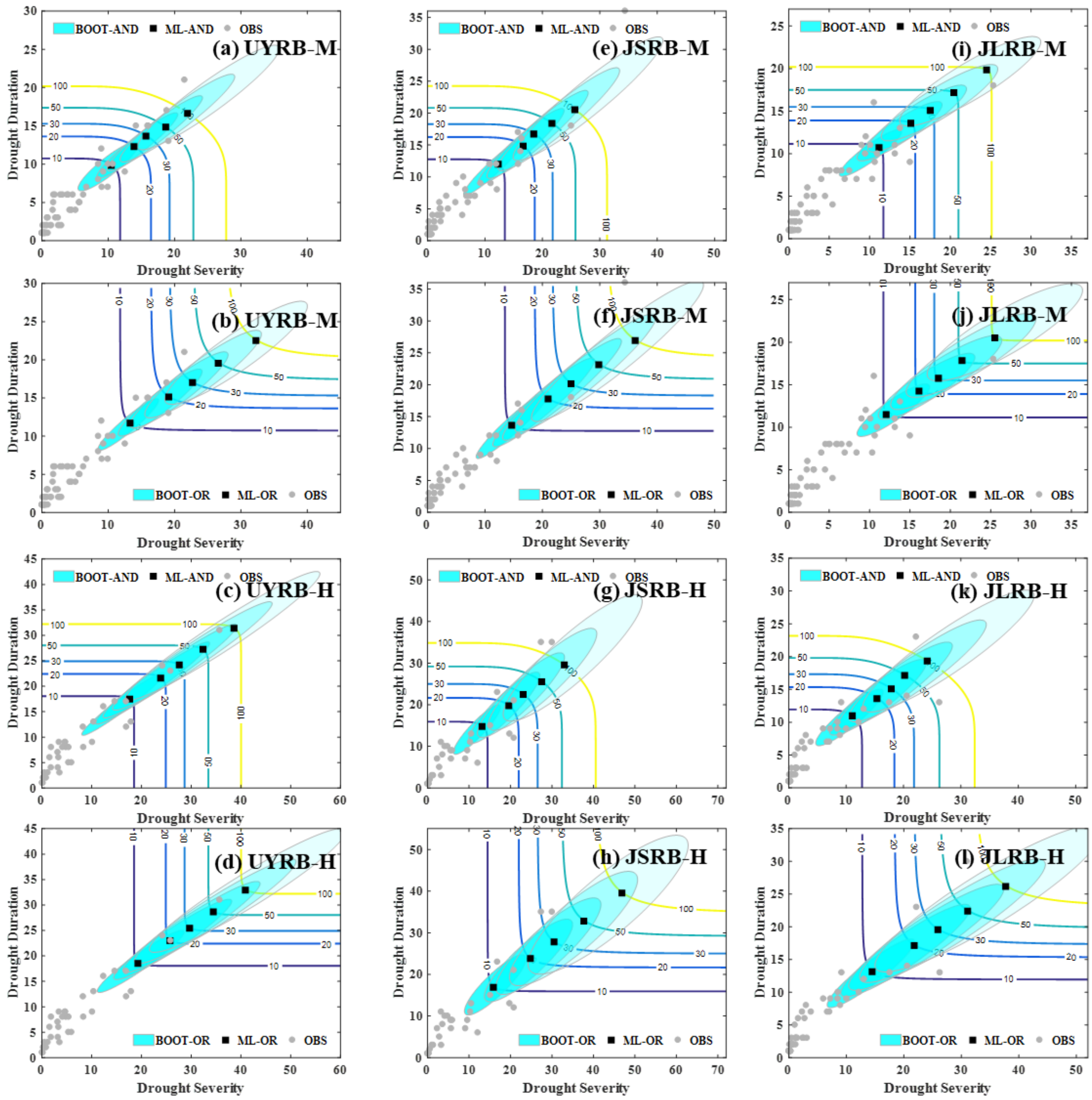

Figure 7 The isolines, bivariate quantiles and 95% confidence ellipse of drought duration and severity for the meteorological droughts (M) and the hydrological droughts (H) in the three catchments. The isolines are associated with 10-, 20-, 30-, 50- and 100-year return periods, respectively.

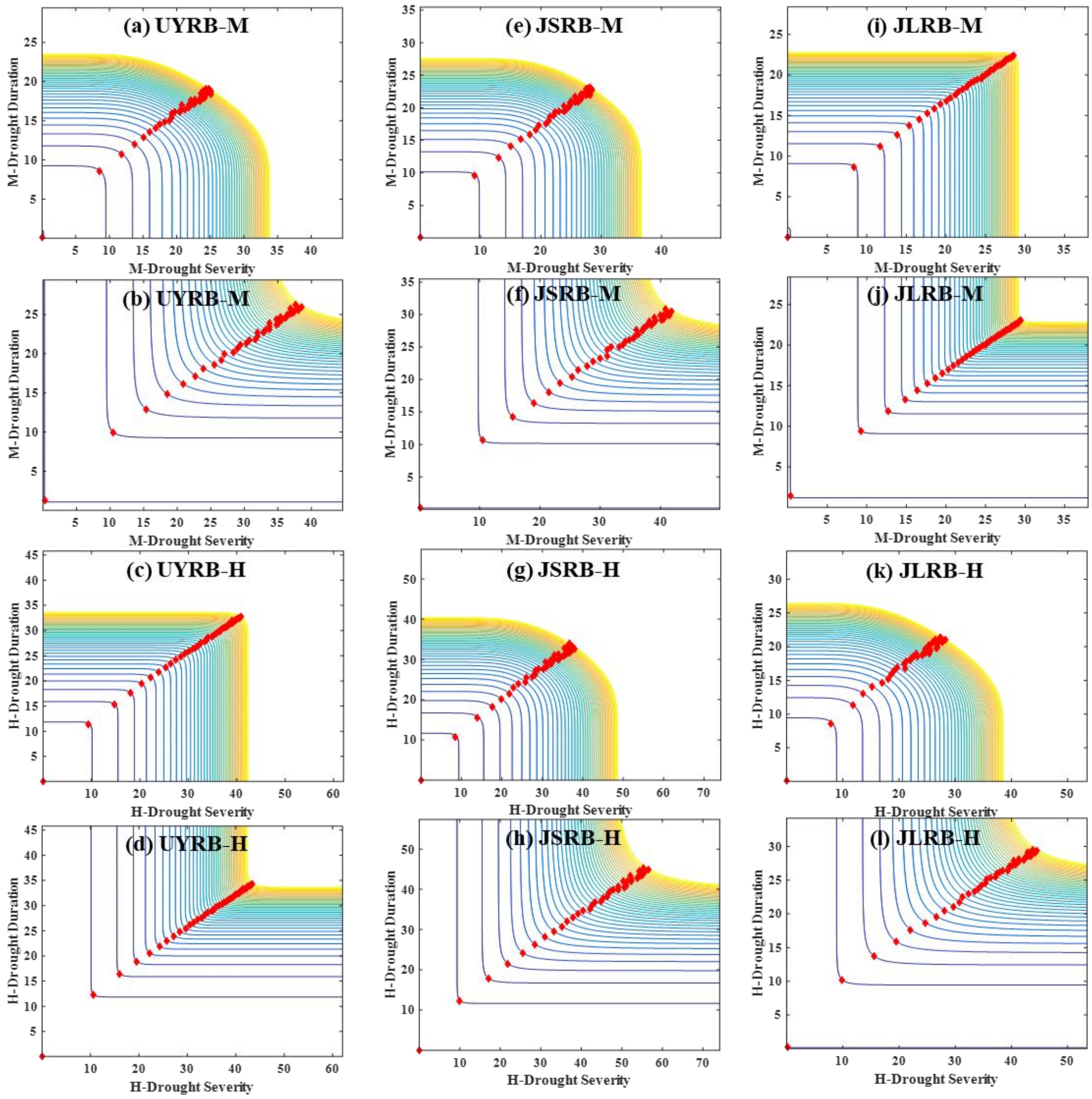

Figure 8 The isolines, bivariate quantiles of drought duration and severity ranging from 10-year to 200-year return periods (under the 5-year intervals) for the meteorological droughts (M) and the hydrological droughts (H) in the three catchments.

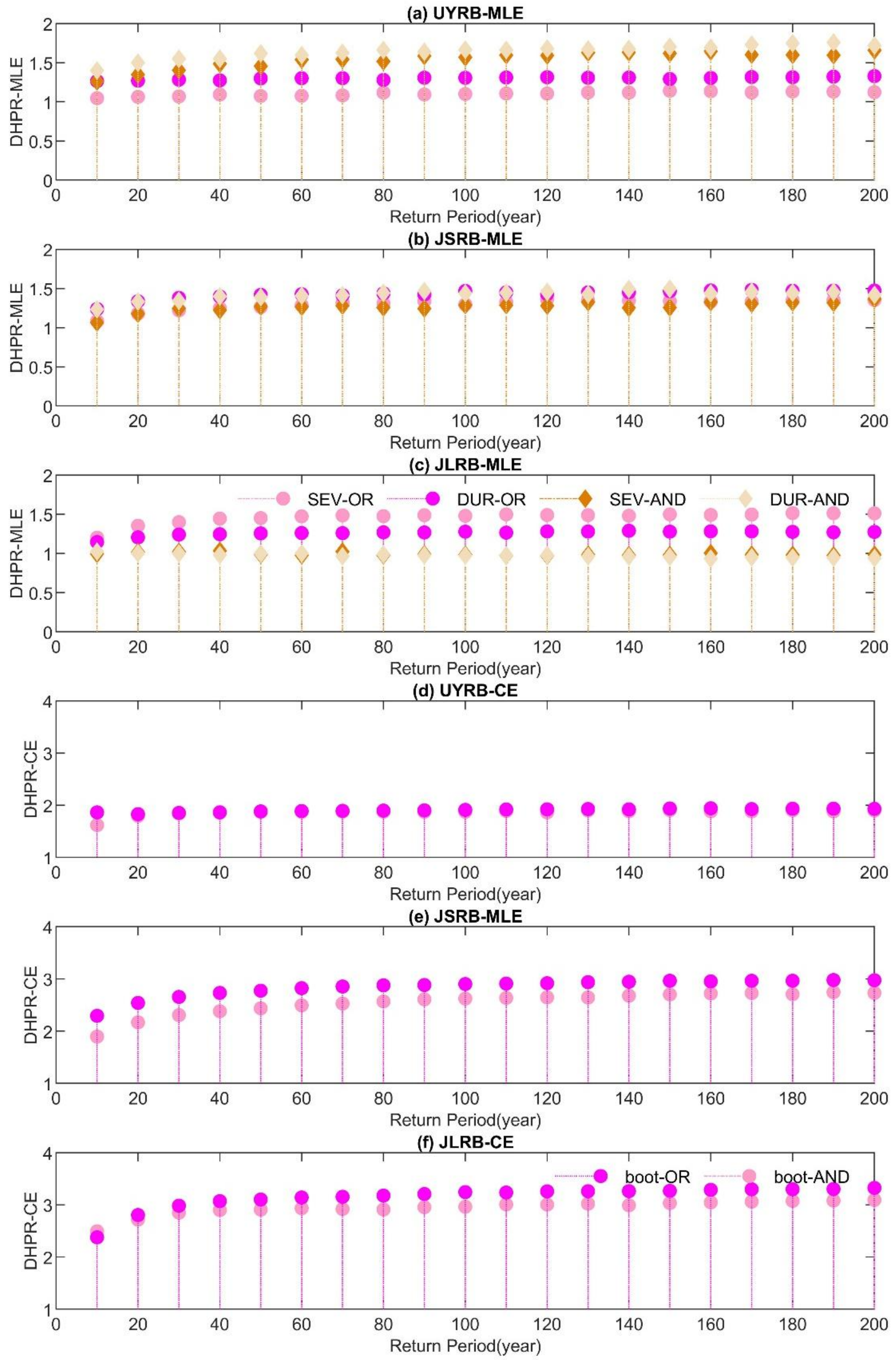

Figure 9 DHPR-MLE and DHPR-CE of drought duration and severity ranging between 10-year and 200-year return periods in the OR and AND cases for the three catchments.

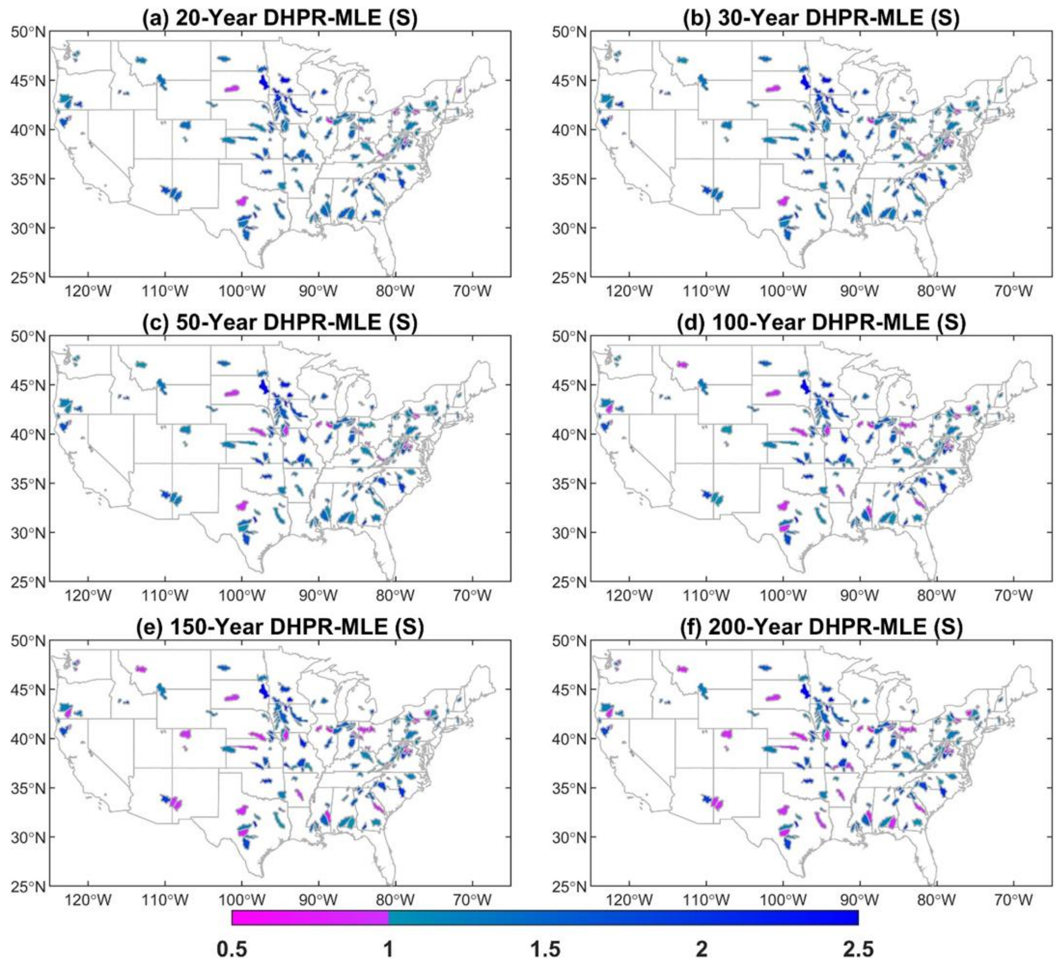

Figure 10 DHPR-MLE under the 20-, 50-, 100-year return periods of severity (S) for 218 catchments in the United States.

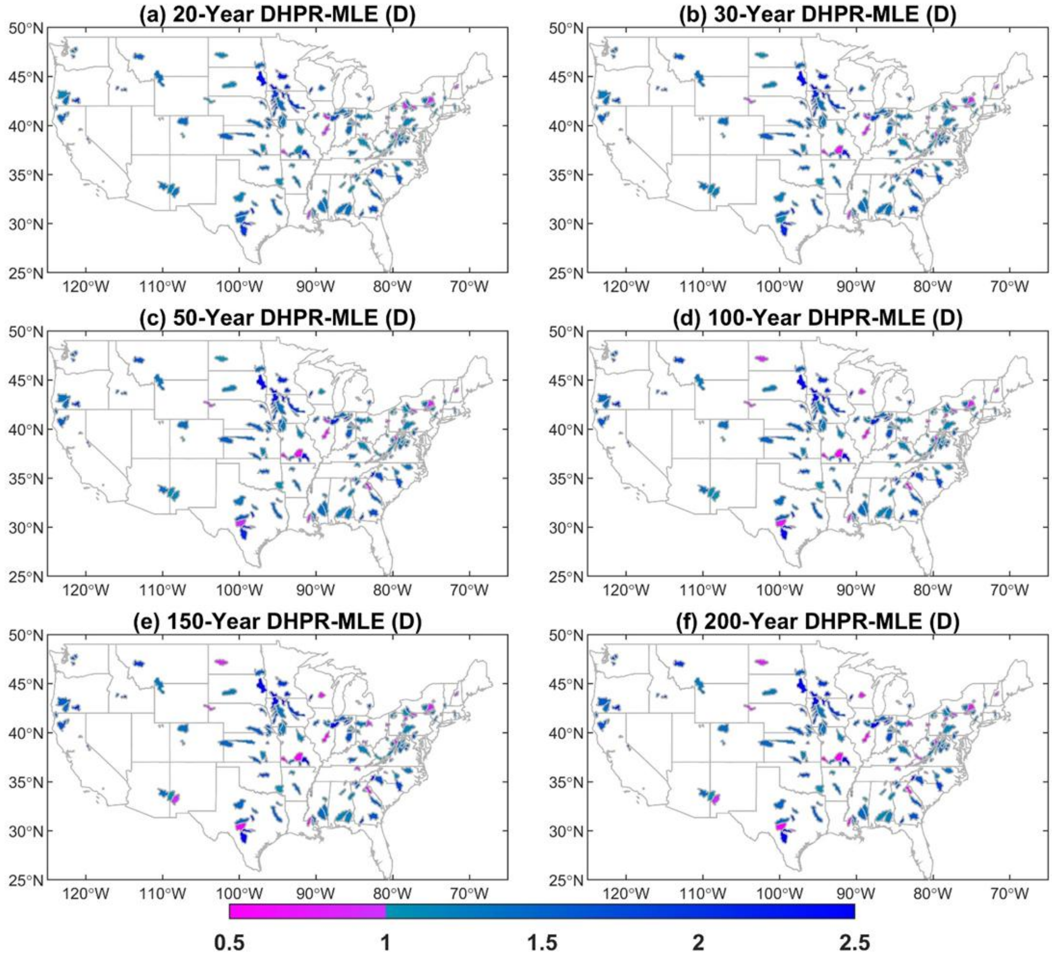

Figure 11 DHPR-MLE under the 20-, 50-, 100-year return periods of duration (D) for 218 catchments in the United States.

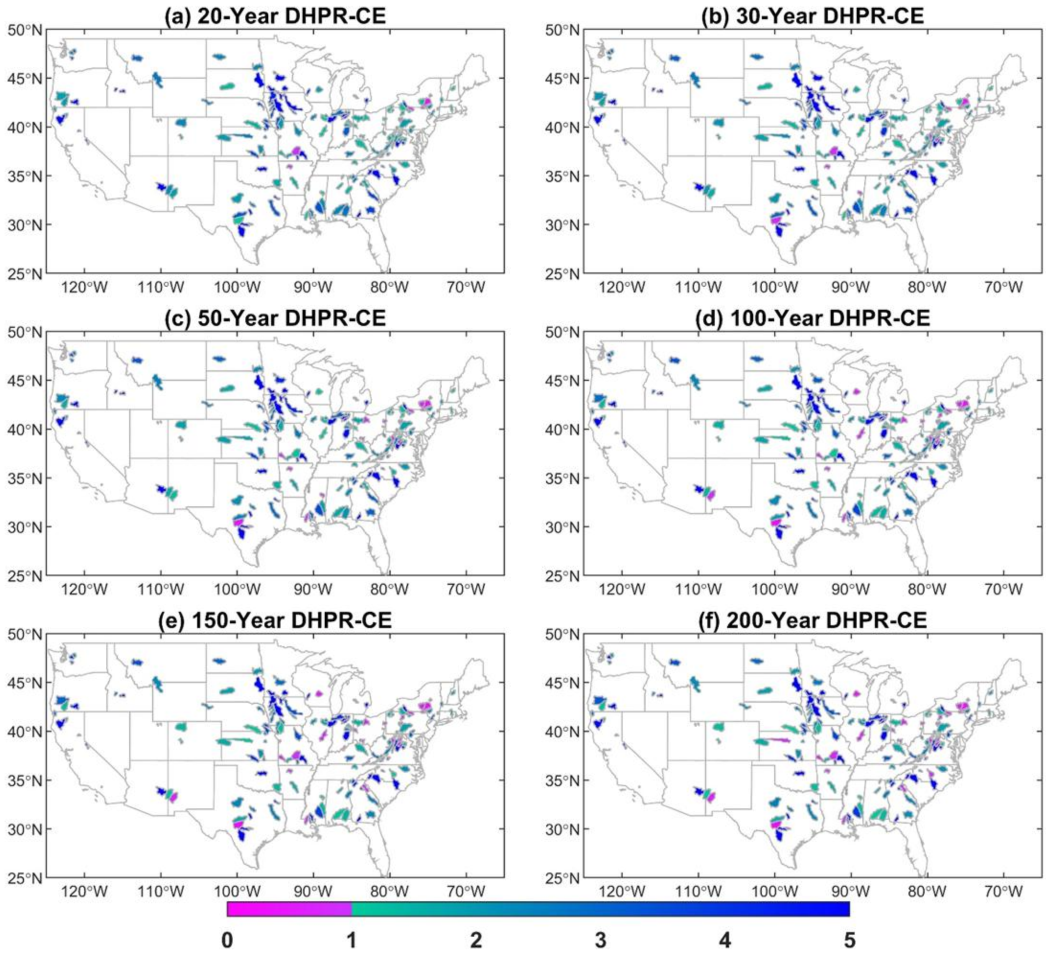

Figure 12 DHPR-CE under the 20-, 50-, 100-year return periods for 218 catchments in the United States.

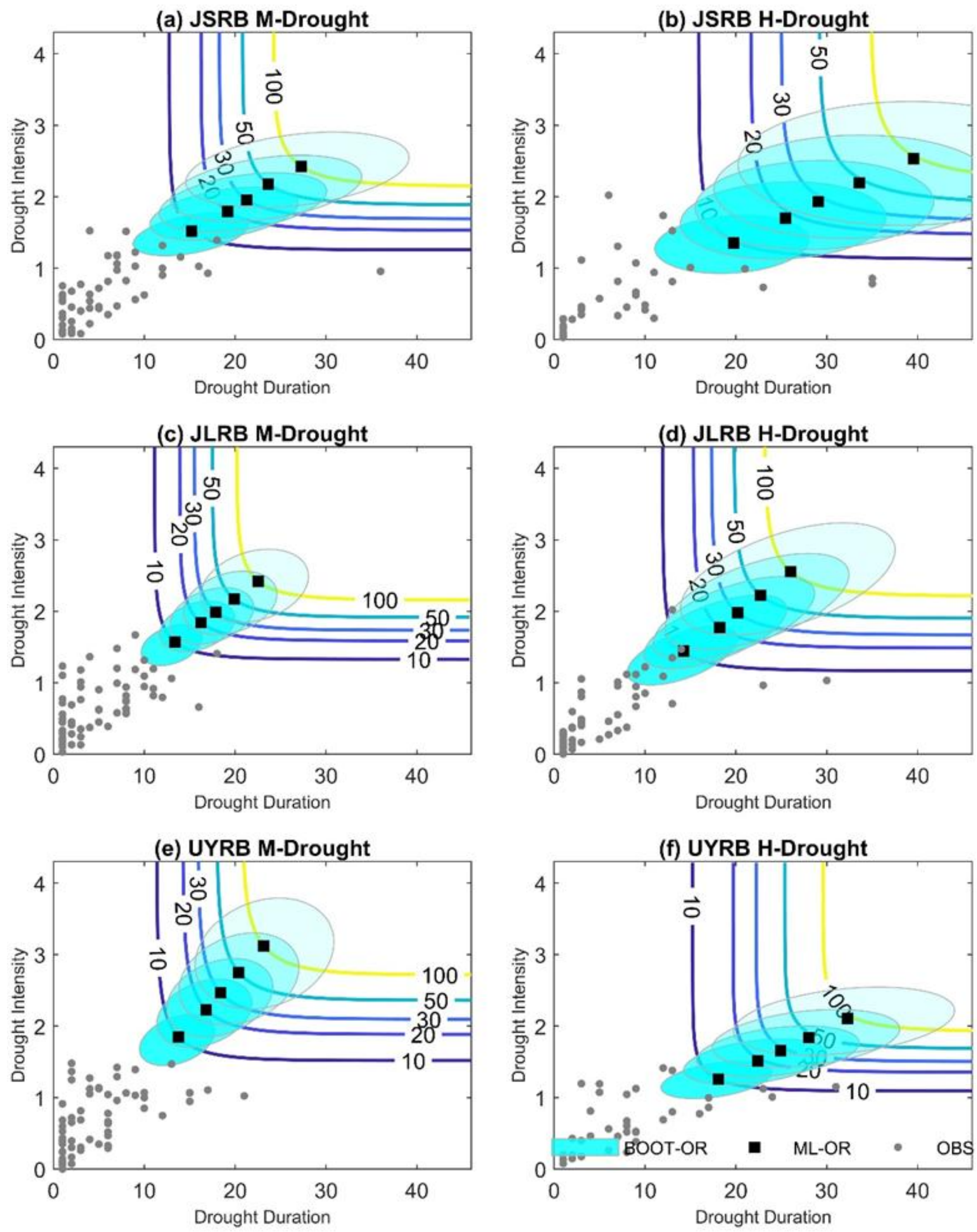

Figure 13 The isolines, bivariate quantiles and 95% confidence ellipse of drought duration and intensity for the meteorological droughts (M) and the hydrological droughts (H) in the three catchments. The isolines are associated with 10-, 20-, 30-, 50- and 100-year return periods, respectively.

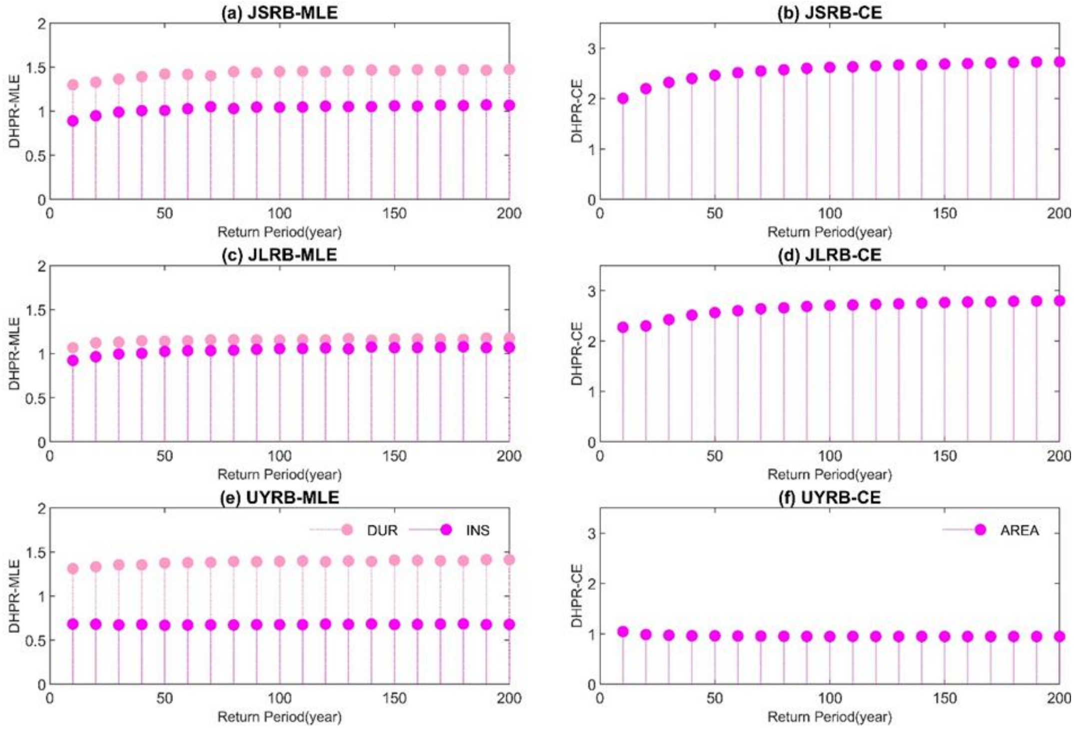

Figure 14 DHPR-MLE and DHPR-CE of drought duration and intensity ranging between 10-year and 200-year return periods in the OR case for the three catchments.

Credit author statement

Jie Chen: Conceptualization; Lei Gu: Data curation, original draft preparation; Jiabo Yin: Visualization, Investigation; Jie Chen and Chong-Yu Xu: Supervision; Lei Gu and Jiabo Yin: Software, Validation; Hua Chen and Chong-Yu Xu: Writing-Reviewing and Editing.

Declaration of Interest Statement

The authors declare that they have no conflict of interest with the work presented here.